Mode propagation in optical nanowaveguides with dielectric cores and surrounding metal layers

Anatoly S. Lapchuk, Dongho Shin, Ho-Seop Jeong, Chun Su Kyong, and Dong-Ik Shin

The mode spectrum in an optical nanowaveguide consisting of a dielectric-core layer surrounded by two identical metal layers is investigated. A simple model based on mode matching to predict the properties of mode propagation in such optical nanowaveguides is proposed. It is shown that quasi-TM_{00} and quasi-TM_{10} modes supported by an optical microstrip line do not have a cutoff frequency, regardless of the size of the metal strips, the thickness of the dielectric slab, and the cross-sectional shape. The transverse size of the TM_{00} mode supported by a nanosized microstrip line was found to be approximately equal to the transverse dimension of the microstrip line. In closed rectangular and elliptical nanowaveguides, i.e., in which all dielectric surfaces are covered with metal films, the cross-sectional shape of the waveguide should be stretched along one side to produce propagation conditions for the fundamental mode.

OCIS codes: 180.5810, 210.4680, 170.0180.

1. Introduction

The spatial resolution of a conventional optical system is limited by diffraction and is approximately equal to half of a wavelength. To overcome this limitation, a scanning near-field optical microscope (NSOM) was designed to produce subwavelength spatial resolution.[1–4] Despite constant efforts to improve its characteristics,[5–13] the NSOM has a poor light throughput because of its small optical transmission through a subwavelength hole at the apex of the probe. A more sophisticated nanostructure than a dielectric probe coated with a metal film with a hole at the apex is needed for obtaining a NSOM with a large throughput. NSOM probes have nanosized elements, with their dimensions controlled to a high degree of accuracy, which makes their fabrication difficult (a special difficulty lies in the fabrication of the metal coating). This difficulty in fabrication of nano objects with specific cross-sectional shapes restricts the progress of NSOM technology.

Theoretical research, unlike experiments, places no restriction on the nanostructures' shapes and hence can be useful for the design of NSOMs with high optical throughput. Previously Lapchuk[14,15] and Lapchuk and Kryuchin[16] proposed using a microstrip probe for the NSOM to significantly improve its optical throughput. However, sufficient theoretical background was not provided, and thus improvements are needed.

The theory of regular waveguides can be a basis for investigation of wave propagation in irregular waveguide structures such as NSOM probes. Although the characteristics of circular optical waveguides are well understood in sufficient detail,[17–20] there have not been many studies of nanosized waveguides with other cross-sectional shapes.[21] Our main purpose in this paper is to investigate the mode spectrum and propagation conditions for nanosized optical waveguides with various cross-sectional shapes that may potentially be useful in NSOM probes. The mode spectrum in an optical nanowaveguide has a complex dependence on structural parameters, optical constants of materials, and the wavelength,[17] owing to a strong penetration of the modal field inside the metal layers and to the surface-plasmon effect, which makes a full investigation of the mode-propagation characteristics of optical nanowaveguides difficult.

As only a few lowest modes play important roles in energy transmission to the aperture in NSOM probes, our investigation is concentrated on these low-order modes only. As there is no commercial software that can be directly applied to solution of the eigenvalue problem under study as far we know, we

The authors are with the Central Research and Development Institute, Samsung Electro-Mechanics Company, Ltd., Suwon 442-743, South Korea. A. S. Lapchuk's e-mail address is alapchuk@yahoo.com.

Received 5 January 2005; revised 31 July 2005; accepted 2 August 2005.

0003-6935/05/357522-10$15.00/0

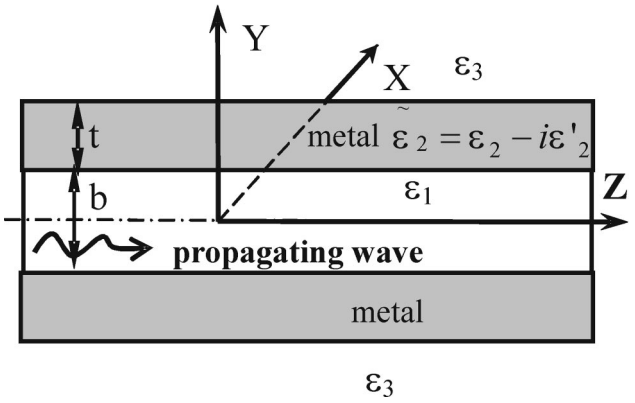

Fig. 1. Schematic of a planar optical nanowaveguide that has a dielectric-core layer surrounded by metal layers.

have developed a simple theory for qualitative understanding of the characteristics of nanowaveguide modes. The eigenmode problem for TM and TE modes propagating in a planar waveguide structure consisting of a dielectric layer surrounded by two identical metal layers is regarded as the key problem in this investigation. The simple assumption for mode interactions with sidewalls, elaborated in microwave theory, was used to predict the properties of propagating modes in nanowaveguides.

A commercial Microwave Studio software package (MWS) based on a finite-integral technique[22–24] (FIT) was used to verify the theoretical results obtained from the simple theory for the microstrip and the rectangular waveguide and to produce additional results for waveguides that have more-complex cross-sectional shapes.

2. Transverse-Magnetic and Transverse-Electric Modes in Planar Nanowaveguides

The modes of planar waveguides are a basis for calculation of the characteristics of three-dimensional waveguide modes in a mode-matching method (MMM). Because the propagation characteristics of modes supportable by planar nanowaveguides[25] and a mathematical method for solution dispersion characteristics[26,27] are well known, we present here only their characteristics that we use hereinafter for the analysis of modes in three-dimensional nanowaveguides. The properties of bulk metals given in Refs. 28 and 29 were used in our numerical simulation.

The geometry of the basic planar optical nanowaveguide structure under study is schematically illustrated in Fig. 1. The waveguide structure consists of a planar dielectric-core layer (with dielectric constant ε_1 and layer thickness a) surrounded by two identical metal layers (with complex dielectric constant $\tilde{\varepsilon}_2$ and layer thickness t). A dielectric medium (usually air) with dielectric constant ε_3, in turn, surrounds the metal layers. The structure is symmetrical with respect to the $y = 0$ plane and, thus, the TM and the TE eigenmode problems can be separated into two independent cases with metal and magnetic walls placed at the symmetry plane.

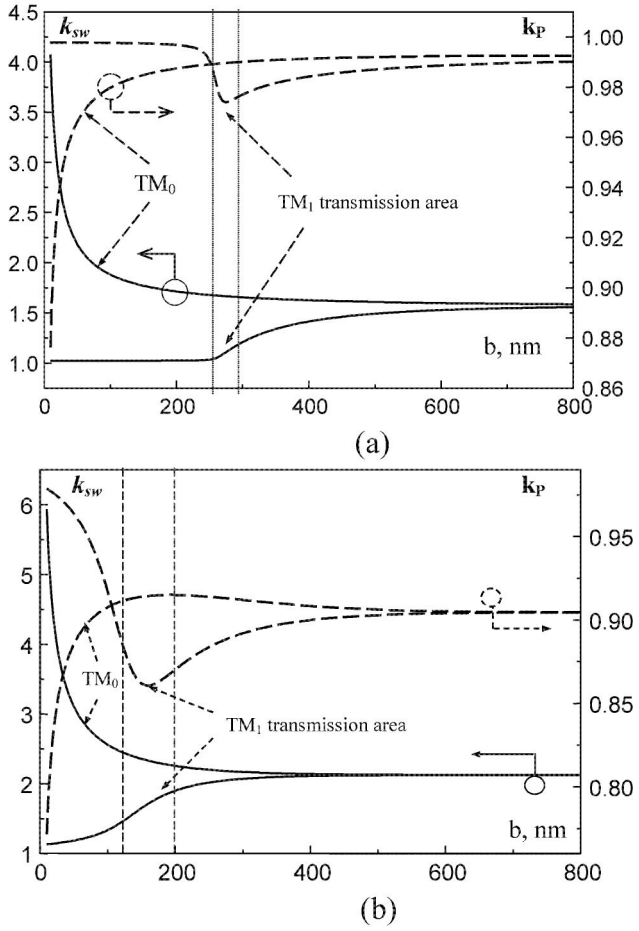

Fig. 2. Slow-wave factor (solid curves) and power attenuation coefficient (dashed curves) of TM_0 and TM_1 waves as a function of the dielectric core's thickness ($\epsilon_1 = 2.25$) for two metal layer thicknesses: (a) $t = 50$ nm and (b) $t = 10$ nm at $\lambda = 780$ nm.

We indexed the waveguide modes according to the values of their wavenumbers (the larger the wavenumber, the smaller the index of the mode) as they are conventionally used in the two-dimensional waveguide theory.[30,31] Generally, the index of the waveguide mode represents the field dependence on the transverse coordinate. This classification, however, is a little ambiguous because the order of wavenumbers of modes depends on waveguide parameters and can change with changing waveguide parameters.

In the research reported in this paper, attenuation coefficient k_p was used as an indication for power attenuation when a mode is propagating along the waveguide. We define it as $k_P = I_1/I_0 = \exp(-2\alpha s)$, where α is a mode attenuation constant and I_0 and I_1 are the powers of an incident wave and of a wave after propagating along a line interval, respectively. The propagation length was chosen to be 100 nm in the simulation, which corresponds to a typical size of the apex of a NSOM probe.

Figure 2 shows the dependence of slow-wave factor $k_{sw} = \gamma/k$ and power attenuation coefficient k_p for the symmetrical TM_0 and the antisymmetrical TM_1 modes on the thickness of the inner dielectric layer.

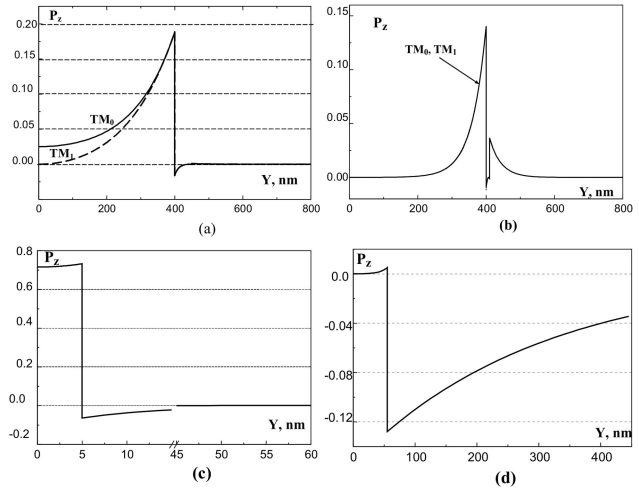

Fig. 3. Power flow distribution (arbitrary units) across the structure with a thickness of the glass layers of $b = 800$ nm for metal coating thicknesses of (a) $t = 50$ nm and (b) $t = 10$ nm. Power flow distribution (arbitrary units) across the structure with a thickness of the glass layers of $a = 10$ nm and a metal layer thickness of the $t = 50$ nm for the (c) TM_0 and the (d) TM_1 modes.

As the thickness of the inner dielectric increases, the slow-wave factor and the attenuation coefficient for two waveguide modes (TM_0 and TM_1) converge to the same value. That is, the TM_0 and the TM_1 waveguide modes are expected to have nearly the same field structure in the limit of large inner-dielectric-layer thickness. As is shown in Figs. 3(a) and 3(b), the electric field exhibits two intensity peaks at the two dielectric–metal interfaces, and its intensity decreases exponentially away from these interfaces. In the center of the inner dielectric layer the electric field intensity becomes close to zero. This means that, for a thick dielectric layer, the TM_0 and TM_1 modes can be represented as even and odd sums, respectively, of two uncoupled surface-plasmon waves propagating along the two metal–dielectric interfaces. The two surface-plasmon waves start to interact with each other if the thickness of the inner dielectric layer becomes smaller than the width of the evanescent tail of the surface-plasmon waves. As the thickness of the dielectric layer decreases, the fields of the symmetric TM_0 mode becomes concentrated in the dielectric and metal layers owing to constructive interference of the two surface-plasmon waves. The field penetration in the metal causes a fast increase of the slow-wave factor and dissipation losses. The field structure of the TM_0 mode for a thin dielectric is nearly homogeneous inside the dielectric layer [Fig. 3(c)], which is similar to the case for fields of a TEM wave between perfect conductor layers. The fields of a TM_1 mode, unlike those of a TM_0 mode, with decreasing dielectric thickness are forced out of the dielectric and metal layers [Figs. 3(b) and 3(d)] in outer space owing to destructive interference of the surface-plasmon waves inside the dielectric-core layer (odd symmetry). This causes the fast decrease of the slow-wave factor [it is approximately 1, as was shown in

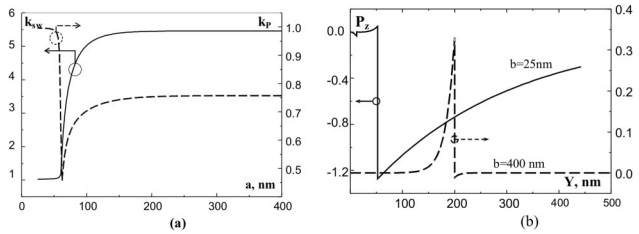

Fig. 4. TM_1 mode parameters of an optical nanowaveguide with a silicon ($\epsilon_1 = 13.7$) and a 40 nm thick silver coating layer at $\lambda = 780$ nm: (a) slow-wave factor (solid curve) and power attenuation coefficient (dashed curve) as functions of dielectric-core thickness, (b) power flow distribution across the layers for two dielectric-core thicknesses b.

Figs. 2(a), 2(b), and 4(a)] and dissipation losses. The beam width becomes larger than λ [Figs. 3(d) and 4(b)] in this case. As a result the TM_1 mode is transformed (for the case of a large dielectric thickness) into an antisymmetrical slow wave propagating along the metal–air interface. Therefore (because of transmission of the field intensity peaks from the inner metal–dielectric layers to the outer metal–air regions) the TM_1 mode has a complex nonmonotonic dependence of k_{sw} and k_p on the thickness of the dielectric layer (Figs. 2 and 4).

The TM_2 mode is a symmetrical surface-plasmon wave propagating along the outer metal–dielectric (air) interface with a small field penetration inside the dielectric layer, as is shown in Figs. 5(b) and 5(c). The abrupt change in the slow-wave factor and the power attenuation coefficient of the dielectric layer's thickness [Fig. 5(a)] may be due to the resonance in the dielectric layer [see the field distribution in Fig. 5(c)]. The symmetrical TM_2 wave does not exhibit

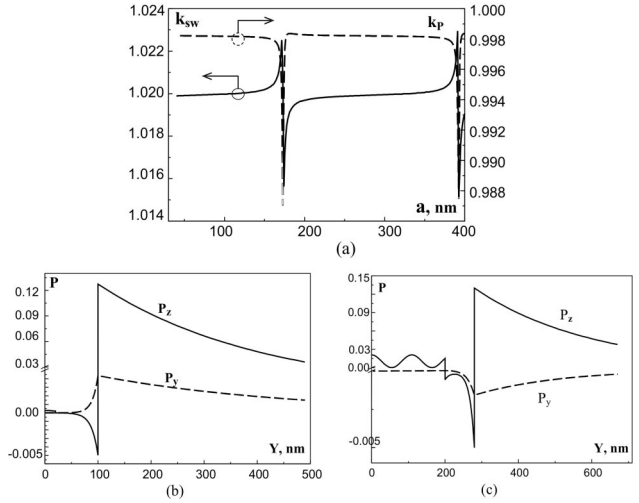

Fig. 5. Propagation characteristics of the TM_2 mode for a planar-optical nanowaveguide with a silicon ($\epsilon_1 = 13.7$) core and 80 nm thick silver coating layers at $\lambda = 780$ nm. (a) Slow-wave factor (solid curve) and power attenuation coefficient (dashed curve) as a function of the thickness of the silicon core layer. Power flow distribution along layers P_z and P_y for core thicknesses of (b) $a = 20$ nm and (c) $b = 400$ nm.

cutoff and remains a slow wave for a small dielectric thickness. The TM_2 mode, similarly to the TM_1 mode, has a slow-wave factor close to 1 and a large cross-sectional beam size.

Analysis of TE modes has shown that their field structures and dispersion characteristics, as for a circular waveguide,[17] are similar to those of conventional TE waves in a microwave band [with a cutoff dielectric-layer thickness approximately equal to $m\lambda/(2n)$, where n is a positive integer]. The only difference is that modes are transformed into leaky waves (radiated modes) with decreasing dielectric-core layer thickness rather than being evanescent as they are in the microwave regime, owing to transparency of the waveguide walls.

3. Optical Microstrip, Rectangular, Circular, and Elliptical Waveguides

The MMM is often used in microwave theory[32–34] for calculation of the characteristics and fields of waveguide modes for a waveguide with a stepwise constant refractive-index profile. There are three steps in the solution of an eigenmode problem by the MMM. First, for each slab, one has to write the field of the mode as a sum of physically reasonable fundamental solutions of the wave equation (the field of the plane waveguide mode). Second, the continuity requirements for the electromagnetic fields must be incorporated to connect the unknown coefficients on neighboring slabs, resulting in a system of linear equations. Third, this system has to be solved for a nonvanishing field.

The MMM commonly is applied for solution of eigenmode problems for closed waveguides. The modes of the plane waveguide form a complete set of functions for the area inside the closed waveguide, and this fact is the basis of the MMM. For an open structure such as a microstrip line the MMM should be modified because the set of eigenmodes of a plane structure is not complete for an infinite area. The simplified MMM is usually used in the microwave band for a microstrip line for engineering calculation. The simplified MMM is based on the assumption that only one mode of a plane waveguide is essential for calculation of the basic mode of a microstrip line.[32–34] Knowledge of the reflection coefficient of this mode from the side waveguide's walls is needed for using the simplified MMM to find the solution of the eigenmode problem. Calculation of the reflection coefficient of the plane waveguide mode from the plane structure end (from the microstrip sidewall) is a complex exercise that often is handled separately from the eigenmode problem.[35] Often in microwave theory the magnetic sidewall model (with appropriate change of waveguide width and dielectric constant to effective ones) is used for the calculation of the basic quasi-TM_{00} mode.

The nanowaveguides in an optical wave band are open structures because of partial penetration of the electromagnetic field through the nanometer metal layer in the optical wave band, and therefore a simplified MMM and indirect eigenmode calculation with the MWS are used here for obtaining the characteristics of the modes of the nanowaveguide.

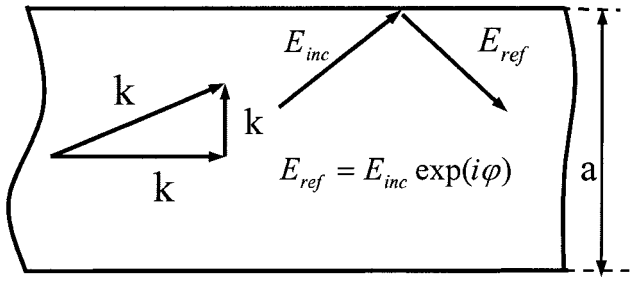

Fig. 6. Schematic of a simplified mode-matching method.

The condition for a wave of plane structure to create a waveguide mode by reflection from the structure's two sidewalls (see Fig. 6) can be written by use of the phase of the reflection coefficient (from the waveguide sidewall) as follows:

$$2k_x a + 2\varphi = 2n\pi, \tag{1}$$

from which a dispersion equation can be obtained by

$$k_x = (n\pi - \varphi)/a\,,$$

$$k_z = (k_{s1}^2 - k_x^2)^{1/2}, \tag{2}$$

where k_{s1} is the wavenumber of the planar waveguide; k_x and k_z are the x and z components, respectively, of k_{s1}; n is the waveguide-mode index along the x axis; and ϕ is the phase of the reflection coefficient. Using the simplified MMM reduces the complex problem of field propagation in a nanowaveguide to a simple problem of mode propagation in a planar structure and to calculation of the phase of the reflection coefficient from the sidewall.

Although many types of microstrip line are used in a microwave technique,[35,36] we are interested mainly in the simplest form of a microstrip line in the optical regime, as shown in Fig. 7. This optical microstrip consists of a rectangular dielectric rod coated with thin metal strips on the upper and lower surfaces. As was shown above, for an optical wave band the TM_0 wave propagating in a thin dielectric layer covered with two metal layers has a field structure similar to that of a TEM wave propagating in a dielectric layer

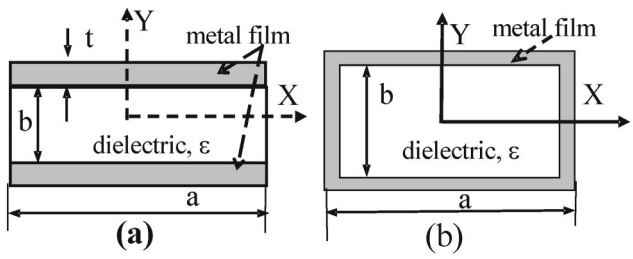

Fig. 7. Schematics of (a) the optical microstrip and (b) the optical rectangular waveguide under study.

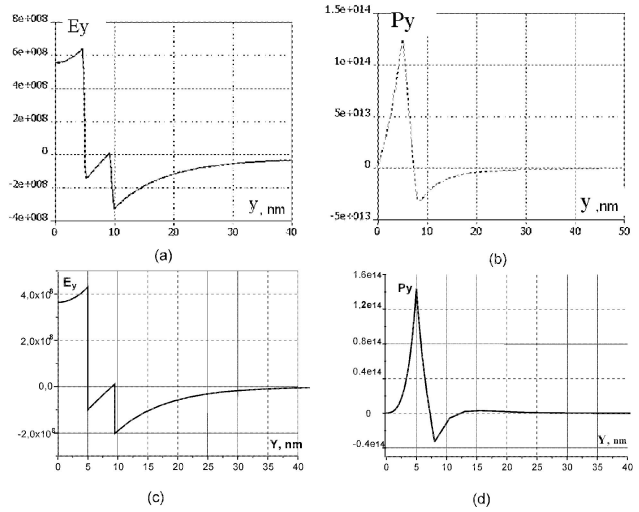

Fig. 8. Comparison of the mode parameters calculated by the MWS and by an analytical model for the TM_0 mode supported by a plane waveguide structure with a 10 nm thick dielectric-core layer ($\varepsilon_1 = 4$) and a 4.5 nm thick silver coating layer at $\lambda = 650$ nm: (a) electric field component E_y (arbitrary units), (b) power flow P_y (arbitrary units) calculated by the MWS; (c) electric field component E_y (arbitrary units), (d) power flow P_y (arbitrary units) calculated by the analytical model.

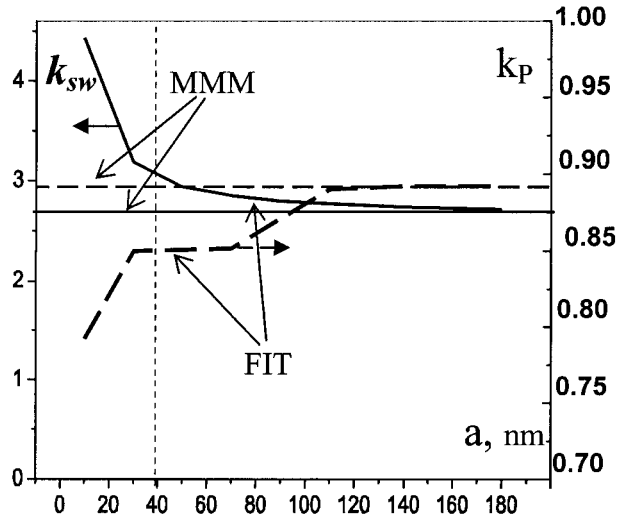

Fig. 9. Slow-wave factor (solid curve) and attenuation coefficient (dashed curve) of the quasi-TM_{00} mode as a function of microstrip width. The microstrip has a core layer ($\epsilon_1 = 2.25$) and 20 nm thick silver metal strips with a length of $b = 40$ nm operating at $\lambda = 790$ nm.

surrounded by perfectly conducting metal plates. A model for a microstrip optical probe[14–17] that used the similarity of the field structures of the fundamental modes of microstrip lines in microwave and optical wave bands was proposed, and it was shown that a significant improvement in optical throughput, compared with that for a conventional probe, and a strong field enhancement were achievable. As was found above, however, some parameters of the TM_0 mode in the optical band are significantly different from those of the TEM wave owing to strong field penetration in metals. In addition, unlike for the ideal metal layers, there are also other types of mode that can propagate in a thin dielectric layer between two metal layers (TM_1 and TM_2, for example) in an optical band, which can cause the accuracy of the simple model in an optical wave band to deteriorate. Therefore this approach should be verified either by a rigorous solution of the waveguide problem (indirect calculation with the MWS, for example) or by an experiment.

We used the TM_0 wave parameters obtained from the analytical solution to test the accuracy of the FIT in the optical wave band (see Fig. 8). Because the MWS does not provide direct eigenmode solutions for a medium with high losses (as it does for an optical wave band) we used a long section of a homogeneous line and a quasi-TEM wave (fundamental microstrip mode), incident from a microstrip line that had perfectly conducting metal strips, to excite our structure to obtain TM_0 wave parameters. We used a microstrip region far from the junction to extract mode parameters of the optical microstrip. It should be noted that, owing to the symmetry of the structure and to the field excitation, the field in the far region could be represented as a superposition of TM_0 and TM_2 modes, which can decrease the accuracy of data obtained for the TM_0 mode. Nevertheless, the field patterns in the far region obtained by numerical simulations are in good agreement with those from the analytical solution for the TM_0 mode (Fig. 8). This may be due to weak coupling between the incident TEM mode and the TM_2 waves, which have different field structures. Numerical comparison has shown that wavenumbers and dissipation losses obtained by the two methods agree well, with errors within 1.5% and 3.2%, respectively. This level of error is within the accuracy of the method, which was applied to extract the mode parameters from the numerical results.

We are interested mainly in a few first quasi-TM_{nm} modes, which can propagate in the region near the probe apex of the NSOM, where the first subscript, n, denotes the field dependence on the x axis (coordinate across the layer) and the second subscript, m, on the y axis (along the layer in the microstrip's cross section). It should be noted that, for a complex structure such as a microstrip line, this notation is somewhat ambiguous because of the complexity of the field structure of microstrip modes. For small microstrip sizes, however, only a few waves can propagates in the line. The properties of these modes are assumed to be derivable from the properties of the TM_n waves propagating in the infinite two-dimensional dielectric–metal-layer structures analyzed above, and thus our notation for the microstrip mode is based on this fact.

We used the excitation of a nanowaveguide by the field of a mode of a microstrip line with perfectly conducting strips in all cases of nanostructure excitation described below. Figure 9 shows the characteristics of a fundamental quasi-TM_{00} microstrip mode calculated by the rigorous FIT algorithm and by the

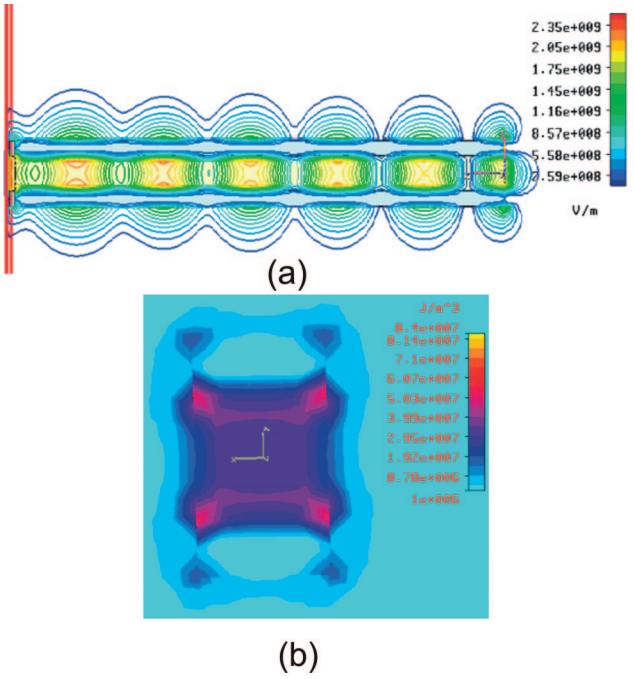

Fig. 10. (a) Electric field amplitude of the quasi-TM_{00} mode along the microstrip line (at $X = 0$) and (b) electric field energy density at the cross section (at $z = 30$ nm) in a microstrip line with length $s = 160$ nm covered with silver metal strips: $a = b = 10$ nm, $t = 4.5$ nm, $\epsilon_1 = 4$, $\lambda = 650$ nm ($\gamma/k = 14.0$ and $k_P = 0.565$ calculated by the FIT and $\gamma/k = 12.4$ and $\kappa = 0.503$ for a rigorous two-dimensional algorithm).

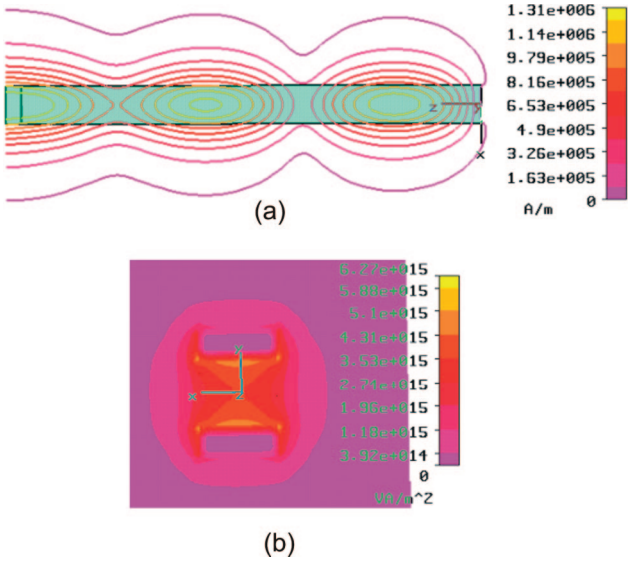

Fig. 11. (a) Magnetic field amplitude of the quasi-TM_{00} mode along the microstrip (at $Y = 0$). (b) Power flow (z components) at the microstrip cross section (at $z = 20$ nm) in an optical microstrip line with length $s = 60$ nm covered with gold metal strips: $a = b = 5$ nm, $t = 1.5$ nm, $\varepsilon_1 = 4$, $\lambda = 1520$ nm.

simplified MMM in which the waveguide sidewalls are replaced by magnetic walls ($\varphi = 0$, $n = 0$). The simplified MMM with magnetic sidewalls measures any dependence of the slow-wave factor and the attenuation coefficient on microstrip width (TEM mode approximation), whereas a rigorous FIT model gives a sharp increase in the slow-wave factor for a narrow ($a < b$) microstrip line. The difference between mode characteristics calculated by the two methods decreases quickly with increasing microstrip width and approaches zero. For a wide microstrip line ($a > b$) the characteristics of quasi-TM_{00} modes (a slow-wave factor and an attenuation coefficient) obtained by both methods agree well. Note that the slow-wave factor and the attenuation calculated by the FIT are always larger than those obtained by the MMM. Figure 10 shows the electric field amplitude and the energy density distribution of the quasi-TM_{00} mode of the microstrip line. One can see that the cross-sectional size of the quasi-TM_{00} field is approximately equal to the size of a microstrip's cross section. From the electric field distribution in Fig. 10 one can see that it has large peaks at the metal strip ends, with large field penetration into the metal. It is these field intensity peaks in the areas of the metal edges that make the slow-wave factor and the attenuation coefficient of the TM_{00} mode of the microstrip line larger than those of the TM_0 mode of a planar structure. Therefore the simplified MMM of microstrip lines can be applied only for a qualitative analysis of the characteristics of a TM_{00} mode of an optical microstrip, and a more rigorous model is needed for accurate calculation. It should also be noted that the electric field of the fundamental mode of an optical microstrip has a loop of an electric field near the microstrip end, similar to that for the conventional microstrip line [Fig. 10(a)].

As the width of the fundamental mode of an optical microstrip is approximately equal to the microstrip line's transverse structure size, one can expect that it will be possible to obtain a beam of a few nanometers' size for a tiny microstrip. In Fig. 11 a field pattern with a beam size smaller than 10 nm propagating in a dielectric rod covered with two golden strips is shown. This tiny-sized wave has a slow-wave factor as large as 31.1 and a large power loss that is due to strong field penetration in metal.

We use the TM_{10} mode of a microstrip line with perfectly conducting strips (the magnetic plane at $y = 0$) to obtain field patterns of the quasi-TM_{10} mode of an optical microstrip line and that of a rectangular waveguide. The rectangular waveguide consists of a rectangular dielectric rod coated with a metal film, as shown in Fig. 7(b). Figure 11(a) shows a comparison of slow-wave factors for quasi-TM_{10} modes of a rectangular waveguide and a microstrip line calculated by the FIT (solid curves) and by the MMM (dashed curves). Phase ϕ of a reflection coefficient for the MMM was obtained from Eq. (2) by use of k_z calculated by the FIT. This phase was calculated only for one microstrip width, and then this value was used for calculation of the dependence of the mode's slow-wave factor and attenuation coefficient on the microstrip's width. One can see from Fig. 12 that even this simple implementation of the MMM (with a constant ϕ) gives a correct dependence of the slow-wave factor

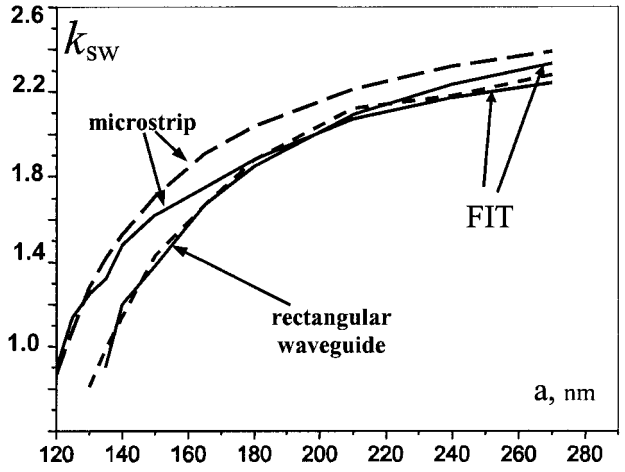

Fig. 12. Dependence of the slow-wave factor of a quasi-TM_{10} mode microstrip line and a rectangular waveguide on the waveguide's width. The structures have a core layer with $\varepsilon_1 = 2.25$ and $b = 40$ nm and silver metal strips with $t = 20$ nm and operating at $\lambda = 790$ nm. Dashed curves, FIT; solid curves, MMM.

on the waveguide's width for calculation of the TM_{10} parameters of an optical microstrip line and a rectangular waveguide.

We used the quasi-TM_{01} mode of a microstrip line with a perfectly conducting metal strip (magnetic plane at $y = 0$) with the same transverse sizes for the excitation of the quasi-TM_{01} mode in an optical microstrip line and a rectangular waveguide. Figure 13(a) shows the electric field pattern of a quasi-TM_{01} mode for a tiny optical microstrip line. Similarly to the TM_1 field of a plane structure, the peak of the field intensity of this mode for a small dielectric thickness is located outside the dielectric layer. However, this mode has a significantly larger slow-wave factor than

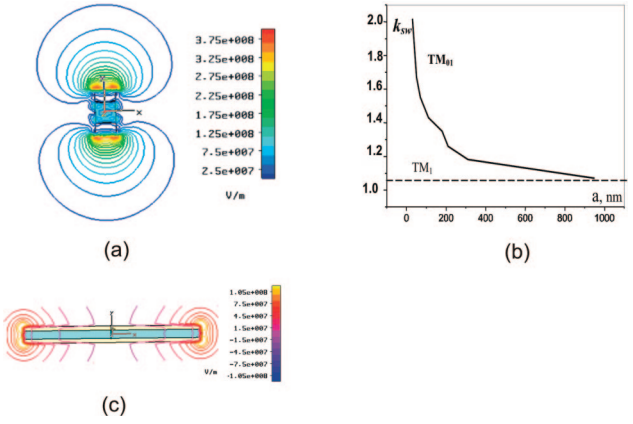

Fig. 13. (a) Electric field distribution E_y of the quasi-TM_{01} mode at a microstrip cross section. The microstrip parameters are $a = b = 10$ nm, $t = 5$ nm (silver), $\varepsilon_1 = 2.25$, and $\lambda = 780$ nm ($k_{sw} = 6.0$). (b) Dependence of the slow-wave factor on the TM_{01} mode of the microstrip linewidth: $b = 40$ nm, $t = 20$ nm (silver), $\varepsilon_1 = 2.25$, and $\lambda = 770$ nm. (c) Electric field amplitude $|E|$ of the quasi-TM_{01} mode at a microstrip cross section: $b = 40$ nm, $a = 850$ nm, $t = 20$ nm (silver), $\lambda = 770$ nm.

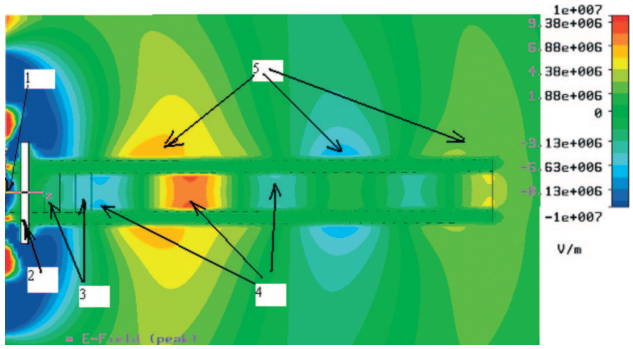

Fig. 14. E_y field distribution of the quasi-TM_{02} mode along the microstrip line with silver metal strips at the $x = 0$ plane. The microstrip parameters are $a = b = 100$ nm, $t = 30$ nm, $\varepsilon_1 = 2.25$, and $\lambda = 780$ nm: 1, microstrip with perfectly conducting metal strips; 2, perfectly conducting rectangular plate; 3, slabs with large absorption; 4, loops of the electrical field of the quasi-TM_{00} wave; 5, loops of the electrical field of the quasi-TM_{02} wave.

the TM_1 mode of the plane structure, as shown in Fig. 13(b), a fact that can be explained as follows: The field of the TM_1 mode of the plane structure has a small-field penetration in the metal of a waveguide of small dielectric thickness. The electric field has a large intensity at sharp metal ridges. As a result of these two effects the field of a quasi-TM_{01} mode is concentrated at the edges of the metal strips (with a strong penetration into the metal), and therefore for narrow metal strips the quasi-TM_{10} mode is a ridge mode whose field intensity decreases exponentially with the distance to the edges of the metal strips [Fig. 13(c)]. Rectangular waveguides with field concentration at outer corners of the waveguide exhibit similar TM_{01} behavior. The result is that the quasi-TM_{01} mode has a field structure and other parameters that are significantly different from those of a TM_1 wave of plane structure. However, for significantly large metal strips the edge effect becomes small, and a TM_{01} mode has the same parameters as the TM_1 mode of a plane structure.

We used a complex nanostructure (see Fig. 14) to obtain the field pattern of the quasi-TM_{02} mode, where 1 is a microstrip line with perfectly conducting strips excited by a quasi-TEM wave, 2 is a perfectly conducting plate to reflect the quasi-TM_{00} mode, and 3 marks two plates that have large losses to absorb the rest of the quasi-TM_{00} energy. Despite this large effort to exclude the quasi-TM_{00} mode, the TM_{00} is not completely suppressed, such that the resultant field, as shown in Fig. 14 (where 4 marks the loops of the electric field for the TM_{00} mode and 5, that for the TM_{02} mode), is shown to be a superposition of the TM_{02} and TM_{00} fields. The field pattern of the quasi-TM_{02} mode is similar to that of the two-dimensional TM_{02} mode. Much of this field is distributed in the air rather than in the dielectric and metal layers. The slow-wave factor of the quasi-TM_{02} mode is close to 1. The field structure for a relatively large microstrip line ($a = b = 100$ nm) is shown in Fig. 14.

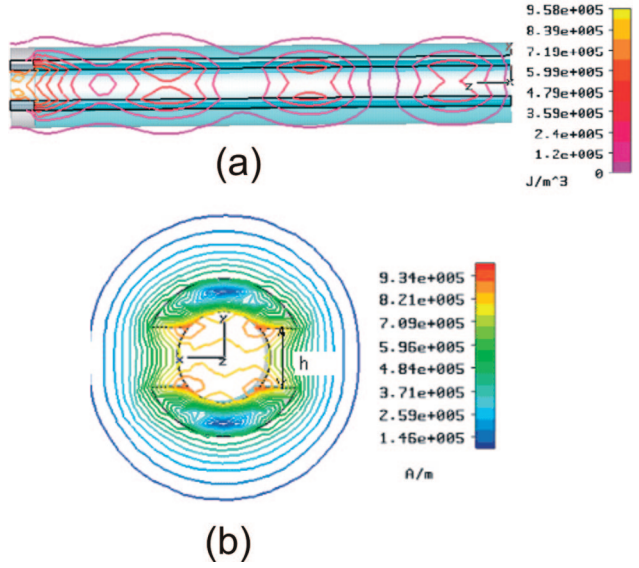

Fig. 15. Field distributions in a microstrip line formed by a circular glass rod with two chord-shaped silver strips placed symmetrically on the upper and lower rod surfaces. (a) Magnetic energy density along the microstrip at $x = 0$. (b) Magnetic field amplitude across the microstrip at $z = 21$ nm. The microstrip parameters are r (rod diameter) 10 nm, $t = 7$ nm, $\varepsilon_1 = 2.25$, $s = 200$ nm, and $h = 1.28r$.

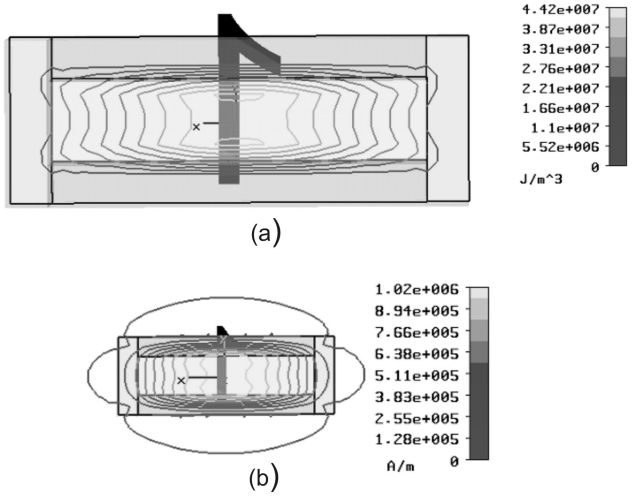

Fig. 16. (a) Electric field energy density at $z = 100$ nm and (b) amplitude of magnetic field H_x at $z = 100$ nm of the fundamental HE_{01} mode for a rectangular waveguide with a silver film coating. The parameters are $\varepsilon_1 = 4$, $b = 36$ nm, $a = 8$ nm, $t = 4$ nm, and $\lambda = 780$ nm.

For smaller microstrip sizes ($a = b = 60$ nm, for example), however, we could not see (despite significant efforts to choose the proper structure) the field of the TM_{02} mode in the field pattern, and thus we assume that this wave becomes cut off.

The fundamental quasi-TM_{00} mode of an optical microstrip can propagate between any two homogeneous metal films stretched along the same axes, as does for microwave frequency. For example, the field structure of the fundamental mode propagating in a microstrip line formed by a circular glass rod covered with two chord-shaped silver strips placed symmetrically at the upper and lower rod surfaces is shown in Fig. 15.

The rectangular waveguide in the microwave regime usually has one side whose length [in Fig. 15(a), for example] is approximately two times that of other side. The TE_{10} mode is the fundamental mode for this waveguide structure, with the electric field polarized along the narrow sidewalls. The cutoff condition for the TE_{10} mode in the microwave band (under a perfectly conducting wall approximation) can be written as

$$\gamma_0^2 = k^2 n^2 - (\pi/a)^2 = 0, \tag{3}$$

where γ_0 is a wavenumber of the fundamental mode and n is the refractive index of a dielectric medium of the waveguide. The rectangular waveguide in the optical region is an open structure, and in an open waveguide only a slow wave can propagate without radiation. Therefore the equation

$$\gamma_0^2 = k^2 k_{sw}^2 - (\pi/a)^2 = k^2 \tag{4}$$

can be used for approximate (small-loss approximation) calculation of the transformation of the rectangular waveguide mode from propagation into a leaky mode. Equation (4) can be applied for approximate calculation of the propagation condition for the fundamental mode of an optical rectangular waveguide by use of the slow-wave factor k_{sw} of the quasi-TM_0 mode of a two-dimensional waveguide. As was found above, the slow-wave factor in an optical wave band can be increased infinitely with a decrease in the thicknesses of the dielectric and metal layers. Therefore one may expect that it will be possible to obtain a propagation condition for a tiny rectangular waveguide (owing to a large slow-wave factor) by proper choice of the waveguide's height and the metal film's thickness. A numerical simulation by MWS showed that this propagation condition is indeed achievable. Examples of field patterns of quasi-TM_{10} modes of a rectangular waveguide are shown in Fig. 16, from which one can see that, even for very thin metal films, the sidewalls are not transparent and can be replaced, with good accuracy, by electric walls. It should be noted that, for providing propagation conditions for a fundamental mode in a tiny optical waveguide, one side of the waveguide should be significantly larger than the other. That is, the waveguide shape should be stretched in a direction orthogonal to the polarization of the electric field.

An elliptical nanowaveguide [a dielectric rod with an elliptical cross-sectional shape whose sidewall is coated with a metal film, as shown in Fig. 17(a)] may be considered a modification of a rectangular nanowaveguide with a smoothly varying height. Therefore one may expect that an elliptical nanowaveguide that has a large eccentricity in its cross-sectional shape will support a propagation mode. From the field pattern of the elliptical waveguide (simulated by the MWS) shown in Fig. 17, one may be able to see that

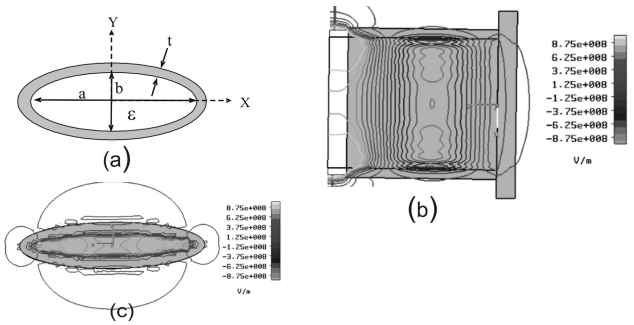

Fig. 17. (a) Schematic of an eliptical waveguide. (b) Electrical (E_y) field distribution along the waveguide at the $y = 0$ plane. (c) Cross-sectional electric field distribution in an elliptical waveguide at the $z = 57.5$ nm plane: $b = 70$ nm, $a = 10$ nm, $t = 5$ nm, $\varepsilon_1 = 2.25$, $s = 80$ nm, $\lambda = 780$ nm.

this simple model works quite well and that several HE_{0m} modes (with different field dependences on x) can propagate in this tiny elliptical nanowaveguide.

4. Conclusions

A simplified mode-matching method and a rigorous finite-integral technique were used to analyze mode-propagation characteristics in optical nanowaveguides. Numerical simulation by both methods has shown the strong correlation between the characteristics of modes of an infinite plane dielectric–metal-layer structure and the characteristics of a nanowaveguide made on the basis of that structure. It was found that the simplified MMM gives correct numerical results for calculation of the dispersion characteristics of a quasi-TM_{01} mode with an error smaller than 10% for microstrip and rectangular nanowaveguides. It was shown that the MMM can be useful for qualitative analyses of the field structure of a quasi-TM_{00} mode of a microstrip and the TM_{10} mode of a microstrip and a rectangular waveguide for a narrow waveguide ($a < b$). It was found that a simplified MMM can be applied for qualitative analyses of the characteristics of the TM_{00} mode of a microstrip line and of the TM_{10} mode of a microstrip and a rectangular waveguide for a wide waveguide ($a > b$).

The application of the MMM is useful in a microwave band, and we hope that it will also be useful in nano-optics. Without any doubt the simplified MMM proposed in this paper needs significant improvement for application in nanowaveguide engineering.

The authors are grateful to Computer Simulation Technology for allowing a trial use of a fully working version of its Microwave Studio software for numerical simulations of three-dimensional nanowaveguide structures.

References

1. E. H. Synge, "A suggested method for extending microscopic resolution into the ultra-microscopic region," Phil. Mag. **6,** 356–362 (1928).
2. E. A. Ash and G. Nicholls, "Super-resolution aperture scanning microscope," Nature **237,** 510–513 (1972).
3. D. W. Pohl, W. Denk, and M. Lanz, "Optical stethoscopy: image recording with resolution $\lambda/20$," Appl. Phys. Lett. **44,** 651–653 (1984).
4. E. Betzig and J. K. Trautman, "Near-field optics: microscopy, spectroscopy, and surface modification beyond the diffraction limit," Science **257,** 189–195 (1992).
5. M. Specht, J. D. Pedarnig, W. M. Heckl, and T. W. Hänsch, "Scanning plasmon near-field microscope," Phys. Rev. Lett. **68,** 476–479 (1992).
6. S. Kawata and Y. Inouye, "Scanning probe optical microscopy using a metallic probe tip," Ultramicroscopy **57,** 313–317 (1995).
7. F. Zenhausern, Y. Martin, and H. K. Wickramasinghe, "Scanning interferometric apertureless microscopy: optical imaging at 10 angstrom resolution," Science **269,** 1083–1085 (1995).
8. J. Silva, S. Schultz, and D. Weller, "Scanning near-field optical microscope for the imaging of magnetic domains in optically opaque materials," Appl. Phys. Lett. **65,** 658–660 (1994).
9. L. Novotny, E. J. Sánchez, and X. S. Xie, "Near-field optical imaging using metal tips illuminated by higher-order Hermite–Gaussian beams," Ultramicroscopy **71,** 21–29 (1998).
10. E. J. Sanchez, L. Novotny, and X. S. Xie, "Near-field fluorescence microscopy based on two-photon excitation with metal tips," Phys. Rev. Lett. **82,** 4014–4017 (1999).
11. J. T. Krug II, E. J. Sanchez, and X. S. Xie, "Design of near-field optical probes with optimal field enhancement by finite difference time domain electromagnetic simulation," J. Chem. Phys. **116,** 10,895–10,901 (2002).
12. T. Nakano, A. Sato, H. Fuji, J. Tominaga, and N. Atoda, "Optical switching property of a light-induced pinhole in an antimony thin film," Appl. Phys. Lett. **75,** 151–153 (1999).
13. E. Oesterschulze, G. Georgiev, M. Müller-Wiegand, A. Vollkopf, and O. Rudow, "Transmission line probe based on a bow-tie antenna," J. Microsc. **202,** 39–44 (2001).
14. A. S. Lapchuk, "Estimation of optical efficiency of a near-field optical microscope on the basis of a simplified mathematical model," J. Opt. A Pure Appl. Opt. **3,** 455–459 (2001).
15. A. S. Lapchuk, "The theoretical investigation of characters of NSOM probe operating on TEM wave," in *Optical Data Storage 2003,* M. O'Neill and N. Miyagawa, eds., Proc. SPIE **5069,** 319–329 (2003).
16. A. S. Lapchuk and A. A. Kryuchin, "Near-field optical microscope working on TEM wave," Ultramicroscopy **99,** 143–157 (2004).
17. L. Novotny and C. Hafner, "Light propagation in a cylindrical waveguide with a complex, metallic, dielectric function," Phys. Rev. E **50,** 4094–4106 (1994).
18. H. Khosravi, D. R. Tilley, and R. London, "Surface polaritons in cylindrical optical fibers," J. Opt. Soc. Am. A **8,** 112–122 (1991).
19. G. C. Aerst, A. D. Boardman, and B. V. Paranjapet, "Nonradiative surface plasmon-polariton modes of inhomogeneous metal circular cylinders," J. Phys. F Metal Phys. **10,** 53–65 (1980).
20. C. A. Pfeiffer and E. N. Economou, "Surface polaritons in a circularly cylindrical interface: surface plasmons," Phys. Rev. B **10,** 3038–3051 (1974).
21. P. Berini, "Plasmon-polariton waves guided by thin lossy metal films of finite width: bound modes of symmetric structures," Phys. Rev. B **61,** 10,484–10,503 (2000).
22. T. Weiland, "Discretization method for the solution of Maxwell's equations for six-component fields," Electron. Commun. **31,** 116–120 (1977).
23. T. Weiland, "Time domain electromagnetic field computation with finite difference methods," Int. J. Numer. Modeling **9,** 295–319 (1996).
24. B. Krietenstein, R. Schuhmann, P. Thoma, and T. Weiland, "Computing eigenmodes in highly lossy accelerating struc-

tures," presented at the XIX International Linear Accelerator Conference (LINAC'90), Chicago, Ill., 23–28 August 1998.
25. H. Raether, *Surface Plasmons on Smooth and Rough Surfaces and on Gratings* (Springer-Verlag, 1988).
26. D. F. Davidenko, "On a certain new method for the numerical solution of systems of nonlinear equations," Dokl. Akad. Nauk SSSR **88,** 601–601 (1953).
27. S. H. Talisa, "Application of Davidenko's method to the solution of dispersion relations in lossy waveguiding system," IEEE Trans. Microwave Theory Tech. **MTT 33,** 967–971 (1985).
28. E. D. Palik, ed., *Handbook of Optical Constants of Solids* (Academic, 1985).
29. D. L. Windt, "Software for modeling the optical properties of multilayer films," Comput. Phys. **12,** 360–370 (1998).
30. L. Wainstein, *Electromagnetic Waves* (Radio and Telecommunications, Moscow, 1988).
31. R. E. Collin, *Field Theory of Guided Waves* (McGraw-Hill, 1960).
32. I. Wolff, G. Kompa, and R. Mehran, "Microstrip band-pass filter using degenerate modes of a microstrip ring resonator," Electron. Lett. **8,** 177–179 (1972).
33. G. Kompa, "S-matrix computation of microstrip discontinuities with a planar waveguide model," Arch. Elektr. Ubertrag. **30,** 58–64 (1976).
34. T. S. Chu, T. Itoh, and Y. C. Shih, "Comparative study of mode-matching formulations for microstrip discontinuity problems," IEEE Trans. Microwave Theory Tech. **MTT 33,** 1018–1022 (1985).
35. A. T. Fialkovsky and E. I. Nefedov, *Microstrip Transmission Lines* (Science, Moscow, 1980).
36. K. S. Gupta, R. Garg, and I. J. Bahl, *Microstrip Lines and Slotlines* (Artech House, 1979).